A meteor radar network study on the polar-to-tropical mesospheric coupling during the 2018 Sudden Stratosphere Warming

S. Eswaraiah [1], Kyong-Hwan Seo[1,2*], Kondapalli Niranjan Kumar[3], Yong Ha Kim[4], M. Venkat Ratnam[5], Evgeny Merzlyakov[6,7], Christoph Jacobi[8], G. Venkata Chalapathi[9], Chalachew Kindie Mengist[10], S. V.B. Rao[11], Nicholas J Mitchell[12] and Neil Hindley[12]

[1] Research Centre for Climate Studies, Pusan National University, Busan, Korea.

[2]Department of Atmospheric Sciences, Pusan National University, Busan, Korea.

[3]National Centre for Medium-Range Weather Forecasting, Ministry of Earth Sciences, India.

[4]Department of Astronomy, Space Science, and Geology, Chungnam National University,

Daejeon, Korea.

[5]National Atmospheric Research Laboratory (NARL), Gadanki, Tirupati, India.

[6]Institute for Experimental Meteorology, Obninsk, Russia.

[7]Kazan (Volga Region) Federal University, Kazan, Russia.

[8]Institute for Meteorology, Leipzig University, Germany.

[9]Department of Physics, Govt. Degree College (A), Anantapur, India.

[10]BK21 School of Earth and Environmental Systems, Pusan National University, Busan, Korea

[11]Department of Physics, Sri Venkateswara University, Tirupati, India.

[12]Department of Electronic & Electrical Engineering, University of Bath, Bath, UK.

Corresponding author: Prof. Kyong-Hwan Seo (khseo@pusan.ac.kr)

Key Points:

- Mesospheric zonal wind reversal with a progressive delay from polar to tropical latitudes appears during SSW.
- Contrasting lateral phase propagation of ISO and high-frequency planetary waves were noted during SSW.
- The dominant ISO, together with weak 8-day planetary waves, favors mesospheric wind reversal and its delay.

Abstract

Using advanced meteor radar network observations along with ERA5 data, we report observational evidence of polar to tropical mesospheric teleconnections during the 2018 major sudden stratosphere warming (SSW) event in the northern hemisphere. A peak SSW on February 14, 2018, characterized by a ~ 45 K rise in polar stratosphere temperature and a zonal wind reversal of ~ (–25) m/s at 60°N and 10 hPa, is observed. In the tropical lower mesosphere, a maximum zonal wind reversal (–24 m/s) compared with that identified in the extra-tropical regions was observed. Moreover, a time delay in the wind reversal between the tropical/polar stations and the mid-latitudes was detected. The wind reversal in the mesosphere is due to the propagation of dominant intra-seasonal oscillations (ISOs) of 30–60-days and the presence and superposition of 8-day period planetary waves (PWs). The ISOs phase propagation is observed from the high- to low-latitudes (60°N to 20°N) in contrast to 8-day PWs phase propagation, indicating the change in the meridional propagation of winds during SSW. However, the superposition of dominant ISOs and weak 8-day PWs could be responsible for the delay of the wind reversal in the tropical mesosphere. Therefore, this study has strong implications for understanding the reversed (polar to tropical) mesospheric meridional circulation during SSW.

Keywords: Sudden Stratospheric Warming (SSW), Tropical-Extra-Tropical Mesosphere, Meteor Radar Network, Mesosphere Wind Reversal, Intra-seasonal Oscillations (ISO), Planetary Waves (PWs), Mesosphere Circulation.

1 Introduction

Sudden stratospheric warming (SSW) (Baldwin et al., 2021) is one of the most remarkable and extreme atmospheric phenomena which occurs in the boreal winter, causing the polar vortex to distort and, at times, even break down (Shi et al., 2017). In recent years, SSW events have attracted significant attention due to their role in changing the earth's middle and upper atmospheric structure and dynamics on a large scale in both hemispheres, thereby affecting the surface weather on a continental scale (Garfinkel et al., 2017; Karpechko et al., 2018), and even influencing the atmospheres of other planets (Pedatella et al., 2018). The mechanism of SSW is well documented (Matsuno, 1971); however, significant ambiguities still exist in its classification (Butler and Gerber, 2018). SSWs occur approximately six times per decade in the northern hemisphere (NH) (Butler et al., 2017; Baldwin et al., 2021). However, due to the weak topographic forcing and smaller planetary wave (PW) amplitudes, SSWs rarely occur in the southern hemisphere (SH) (van Loon et al.,1973), with the exception of the remarkable major SSW event in September 2002 (Krüger et al., 2005) and minor SSW events in 2010 and 2019 (Eswaraiah et al., 2016, 2017, 2018, 2020).

The 2018 SSW that occurred in mid-February in the NH attracted special attention, as it took place after a 4-year gap following the 2013/2014 major SSW. It is the 34^{th} major SSW in the NH counted since 1959 (Fahimi et al., 2021). The favorable climatic factors for the 2018 SSW are specific phases of the quasi-biennial oscillation (QBO) in the tropical stratosphere, the El Niño Southern

Oscillation (ENSO), and Madden Julian Oscillation (MJO) (Butler et al., 2020). The 2018 SSW was registered during the westerly phase of the QBO (wQBO), which favors the development of SSW, however, the coupling mechanism of tropical stratospheric winds to the polar vortex or SSW has not been fully understood (White et al., 2015). Recent studies have proposed that the wQBO allows the propagation of PWs of wavenumber 1 (k=1) (PW1) from the SH into the NH, which is amplified by the QBO and hypothetically contributes to the weakening of the polar vortex and formation of the SSW through enhanced mean meridional circulation (Laskar et al., 2016; Lu et al., 2020). Hence, the SSWs that occur during the wQBO are critical, as they establish the coupling between the tropical and extra-tropical middle and upper atmospheres (Andrews et al., 1987; Laskar et al., 2016,2019). Moreover, during the 2017–2018 NH winter, a La Niña event prevailed, with anomalously cold sea surface temperatures over the eastern and central tropical Pacific Ocean and the tropical Indian Ocean.

In addition, strong MJO phase 6/7 amplitudes were recorded two weeks before the 2018 SSW over the western Pacific (Butler et al., 2020). Another important feature of the 2018 SSW is that this particular event was followed by the canonical weather pattern associated with the negative phase of the Northern Annular Mode for up to two months (Rao et al., 2020), which, in turn, indicates that the downward propagation of the SSW and its surface impacts are greater than those of other events. With these features, the 2018 SSW offers a unique opportunity to extend the current understanding of the middle atmospheric latitudinal coupling and the vertical coupling of the earth's surface climate and atmosphere through the upward propagation of PWs, both in the tropical and extra-tropical regions (Niranjan Kumar et al., 2019; Vargin and Kiryushov, 2019).

Studies related to the latitudinal coupling between the tropical and extra-tropical regions in the middle and upper atmospheres during the NH major SSW events are sparse (Chandran and Collins, 2014; Laskar et al., 2019). Such studies are crucial for an improved understanding of the middle atmospheric mean meridional circulation changes during SSWs. The present study aimed at explaining the changes in circulation during the 2018 SSW. There are several modeling studies that attempt to forecast and characterize the impact of SSW on the lower atmosphere (Rao et al., 2020 and references therein); however, such studies have not been performed for impacts on the middle and upper atmosphere. There are still discrepancies in some models to correctly describe the mesosphere lower thermosphere (MLT) circulation (e.g. Stober et al., 2021). Recently, Satterfield et al. (2022) attempted to resolve errors in the upper atmospheric model using meteor radar (MR) observations.

In addition, studies pertaining to the effects of SSW on the middle atmosphere, especially in the mesosphere, are attained significant importance (Pedatella et al., 2018; Eswaraiah et., 2020). The first observational evidence of a mesospheric response to SSWs was investigated by Quiroz (1969), and many studies have since been carried out in the polar and mid-latitude mesosphere using a vari-

ety of instruments, including radars and model simulations (e.g., Jacobi et al., 2003; Hoffmann et al., 2007; Zülicke and Becker, 2013; Medvedeva et al., 2019; Luo et al., 2021). Responses to SSWs from the low-latitude mesosphere are less reported than in the mid and high latitudes of the NH (Shepherd et al., 2007; Sathishkumar et al., 2009; Eswaraiah et al., 2019). Moreover, the majority of studies on SSW effects in the tropical MLT utilized medium-frequency radar observations at Thumba (8.5°N, 76.9°E), which is very near the magnetic dip equator. Hence, the results might be affected by the equatorial electro-jet (EEJ) (Vineeth et al., 2009). Recently, a state-of-the-art advanced MR has been installed at Tirupati (13.63°N, 79.4°E) a tropical station in India. The Tirupati MR observations have some advantages over other tropical MLT radars, including being unaffected by the EEJ (Rao et al., 2014). Moreover, Eswaraiah et al. (2019) documented the capabilities of the Tirupati MR in detecting mesospheric signatures during a minor SSW, similar to a major SSW. Hence, MR observational studies in the mesosphere obtained a vital reputation.

A few studies have been conducted in the upper atmosphere during the major SSW in 2018. For instance, the mesospheric response was investigated using microwave radiometer measurements (Wang et al., 2019) at a mid-latitude station, in Ukraine (50°N, 36.3°E). Liu et al. (2019) investigated the ionospheric response to the current SSW over the mid and low latitudes. Vargin and Kiryushov, (2019) examined the 2018 SSW impact on the Arctic troposphere, mesosphere, and ozone layer and highlighted the effect of tropical lower atmospheric weather on the current 2018 SSW. To date, no other studies have addressed the mesospheric response to the 2018 major SSW event. At large, the mesospheric response to major SSWs at individual locations/latitudes was well designated over the NH. However, simultaneous ground-based radar observations of the variability of the mesosphere from the tropical to the polar regions and its teleconnections are in high demand but are sparse.

To this end, in the present study, we report the mesospheric response to the 2018 SSW using simultaneous observations from an MR network covering the tropical to the polar regions. By using the advanced MR network and ERA5 (ECMWF Reanalysis-5) datasets, for the first time, we investigate the possible coupling or connection between the tropical and extra-tropical mesosphere via PWs during the 2018 SSW. Data and methodology used in this current study have been given in section 2, the results and discussions are provided in section 3, and the final concluding remarks are summarized in section 4.

2. Data and methodology

We used mesospheric wind measurements from a network of advanced MRs, whose locations are shown in **Fig. 1**. The network of MRs includes Tirupati (TR) (13.63°N, 79.4°E) a tropical station, Collm (CR) (51°N, 13°E) and Kazan (KR) (56°N, 49°E) in the mid-latitudes, and Esrange (ER) (67.88°N, 21.07°E) in the high-latitudes. Because ER is located north of 65.5°N, we considered this station to be in the polar region. All four radars are SKiYMET MRs that function based on the same principle and with a similar setup. The Tirupati MR

(Rao et al., 2014) operates with a peak power of 40 kW at 35.25 MHz, measuring winds from 70–110 km with resolutions of 2 km and 1 h. The Esrange MR operates at 6 kW peak power at 32.5 MHz (Mitchell et al., 2002) and measures winds between 80 and 98 km. The Kazan MR operates with 15 kW power at 29.75 MHz, and the Collm MR operates with a peak power of 15 k at a frequency of 36.2 MHz (Korotyshkin et al., 2019a, b; Jacobi et al., 2019). Both KR and CR measure MLT winds between 80 and 100 km. For the present study, we used the daily mean zonal and meridional winds obtained from MRs from December 1, 2017, to March 31, 2018, at all stations.

To study the SSW characteristics and evaluate PWs, we used ERA5 reanalysis data. ERA5 is the fifth-generation reanalysis data from the European Centre for Medium-Range Weather Forecasts (ECMWF), obtained from the utilization of a 4D-Var data assimilation scheme. ERA5 reanalysis data exhibit higher resolution than ERA-Interim data. The recent ERA5 reanalysis data are made available at a 1-hour time interval with a horizontal resolution of ~31 km (Hersbach and Dee, 2016; Hersbach et al., 2020) and provide atmospheric parameters at 137 levels from the surface to 0.01 hPa (~80 km) (Shepherd et al., 2018; Rüfenacht et al., 2018). The merit of ERA5 data in comparison with existing numerical models and other reanalysis datasets has been discussed by Tarek et al. (2019) and Delhasse et al. (2019).

3. Results and discussions

3.1. SSW event in February 2018 and polar middle atmospheric dynamics

The observed characteristics of the 2018 major SSW and the background dynamical regime of the polar middle atmosphere are displayed in **Fig. 2.** We used ERA5 data to show the disturbance in the polar middle atmospheric temperature, zonal winds, and PWs. **Fig. 2(a)** depicts the time–altitude cross-section of the NH daily mean polar cap (80°–90°N) temperature, and **Fig. 2(b)** displays the daily mean zonal winds at 60°N from December 1, 2017, to March 31, 2018. The approximate heights of respective corresponding pressure levels are displayed on the right axis, and the 10 hPa pressure level is shown by a dashed horizontal line. **Fig. 2(c)** shows the time variability of the PWs of wavenumbers 1 and 2 (k = 1, 2) (PW1 and PW2) obtained at 10 hPa and 60°N. The geopotential heights are used to estimate the PW parameters.

It can be seen from the figure that the cold stratosphere and warm lower mesosphere persist until February 10, 2018 (**Fig. 2a**), and a strong eastward jet (~60 m/s) in the upper stratosphere and lower mesosphere is evident from late December 2017 to January 15, 2018 (**Fig. 2b**). The onset date of SSW is February 11, and peak warming (~45 K) was attained on February 14, 2018 (**Fig. 2a**) with a zonal wind reversal (at about –25 m/s) at 10 hPa and 60°N (**Fig. 2b**). Moreover, the signatures of warming and zonal wind weakening/reversal continued until the end of March 2018. However, previous reports (Karpechko et al., 2018; Wang et al., 2019) have indicated that the onset date of the 2018 SSW

was February 10–12, 2018. **Fig. 2c** reveals that the amplitude of PW1 substantially increased well before (~2 weeks) the onset of the SSW; this increase was responsible for the zonal mean flow reversal, and subsequent deceleration. However, the amplitude of PW2 abruptly increased just before the onset of the SSW, leading to the vortex-split SSW (Vargin and Kiryushov, 2019; Butler et al., 2020). The 2018 SSW is the second-strongest vortex split event, after the 2009 major SSW (Kozubek et al., 2020). We further, noted that the zonal winds during the 2018 SSW largely deviated from the 43-year mean (1979–2021) during the NH winter (figure not shown), exhibiting a stronger (approximately –25 m/s) and longer-lasting wind reversal with an oscillatory pattern. The strong zonal wind reversal in the 2018 SSW is a favorable factor for the downward coupling of the SSW and its higher surface effects (Butler et al., 2020; Rao et al., 2020). However, the role of the tropical climate and its mechanism to induce the weakening of the polar vortex during the 2018 NH winter has not been well reported.

3.2. Tropical and extra-tropical mesospheric mean wind structure

The mesospheric zonal and meridional winds from December 1, 2017, to March 31, 2018, observed by the MR network, are displayed in **Figs. 3a–b**. The panels show the wind field time series from the polar to the tropical regions (from top to bottom). The vertical line in each panel shows the SSW day, and the white patches indicate the gaps in the data. The Tirupati MR (TR) demonstrates its uniqueness in the tropical region by evaluating winds between 70–110 km as a consequence of its high meteor detection rate (Rao et al., 2014; Eswaraiah et al., 2019). Meanwhile, the extratropical MRs at Kazan (KR), Collm (CR), and Esrange (ER) retrieve winds at 80–100 km. Usually, eastward winds (**Fig. 3a**) dominate in the undisturbed winter MLT, both at Esrange (ER) (Mitchell et al., 2002) and at the mid-latitude stations (KR and CR) (Jacobi, 2012); however, in the tropical region, dominant eastward winds exist between 70 and 85 km (Kishore Kumar et al., 2008; Eswaraiah et al., 2019), while above 85 km they are westward. Strong westward winds (wind reversal) were detected during the peak SSW day in the mid-latitudes, and the day after the SSW, they were observed at the tropical and polar stations, continuing for a few days (~2 days over the tropical/polar region and more than 2 days in the mid-latitudes). The episodes of westward winds that exist in the polar MLT (Esrange) before the SSW (December and January) could be caused by the amplification of PW1 (**Fig. 2c**) in the stratosphere and its vertical propagation. After the SSW, the winds turned again eastward. However, a strong and long-lasting wind reversal can be observed in the upper mesosphere (above 90 km) at the mid-latitude stations, whereas the magnitude of the wind reversal is weak in the lower mesosphere (below 90 km). In contrast, in the tropical region, eastward winds are dominant in the lower mesosphere (70–85 km), and the wind reversal (east to west) started in the first week of February (~10 days before the SSW). However, the peak wind reversal occurred two days after the SSW, as the winds returned eastward. In addition, a downward shift in the westward winds has been noted in the tropical region (between 70 and 90 km) before the SSW.

The meridional wind (**Fig. 3b**) structure exhibited an oscillatory pattern before the peak SSW at all stations and diminished afterward. These meridional wind oscillations could be caused by the existence of atmospheric waves of wide periodicities in the background atmosphere. However, strong wind shear was observed from 80–100 km in late December to early January at the ER station. Simultaneously, strong westward winds were observed (**Fig. 3a),** which, in turn, suggests that the westward wind episodes at ER are due to the existence of strong PWs. Wind shears were also noted in the mid-latitudes (KR and CR) at 80–90 km during the day of the SSW. Moreover, the meridional wind oscillations were more significant at the TR (right bottom panel). The meridional winds at TR between 70–95 km show a wide spectrum of wave oscillations before SSW; later, it exhibited the usual seasonal wind pattern (Eswaraiah et al., 2019).

Furthermore, a significant wind reversal is observed in the lower mesosphere below 80 km at the TR station (**Fig.3a**). To determine the lower mesospheric zonal wind structure in the other extra-tropical stations, we obtained ERA5 data near the latitude and longitude of each radar station, as displayed in **Fig. 4.** The figure shows the time–height contours of the daily zonal wind obtained from ERA5 from December 1, 2017, to March 31, 2018, near MR locations. The SSW day is shown as a vertical line. It is worth mentioning that the ERA5 also identified the zonal wind reversal during the day of the SSW at each radar location and showed a delay in wind reversal at the tropical station TR (**Fig. 4d**).

The observed background wind structure in both the tropical and extratropical MLT demonstrated an unusual wind pattern, which could be ascribed to the occurrence of the SSW. A detailed discussion of the variation of the zonal wind and the existence of a wide range of PWs with relevance to the SSW is provided in the following subsections.

3.3. Polar stratosphere–mesosphere connection

To obtain the quantitative differences in the zonal wind reversal at all stations and their connection to the polar stratospheric zonal mean zonal wind, the daily mean zonal winds observed with the MR network in the upper (85–90 km) and lower (78–82 km) mesosphere were averaged and compared with the zonal mean zonal winds at 10 hPa at 60°N from ERA5, as shown in **Fig. 5**. The zonal winds at available altitudes from each station were averaged in the upper and lower mesosphere. The zonal winds in the two mid-latitude stations CR and KR were averaged, whereas the other stations were shown individually.

It is clear from **Fig. 5a** that in the mid-latitudes the upper mesospheric (85–90 km) zonal winds follow the polar stratospheric winds, and the zonal wind reversal started on the onset day of the SSW (February 11), attaining a peak wind reversal (–16 m/s) on the day of the SSW (February 14) (the time of maximum wind reversal in the polar stratosphere). In the polar region (68°N), episodes of westward winds appeared well before the SSW day; which could be

attributed to the upward propagation of PWs in the polar region. However, a peak wind reversal (–18 m/s) occurred two days after the peak SSW (February 16). In the tropical region, typically, the upper mesospheric winds are westward (Kishore Kumar et al., 2008); however, in the present case, the wind reversal (west to east) occurred 10 days before the SSW day (~ February 4) and reached its peak value (~ 28 m/s) one day before the peak SSW event, followed by the weakening of the wind. Wind reversal (approximately −13 m/s)) occurred two days after the SSW day.

Afterward, both the polar and tropical zonal winds abruptly turned eastward as a consequence of the seasonal phenomenon, whereas in the mid-latitudes, they continued until February 23. Briefly, in the mid and high latitude upper mesosphere, a larger wind reversal than in the tropical station was observed, in which mid-latitude (51°–56°N) upper mesospheric zonal winds follow the stratospheric zonal mean zonal wind at 60°N, 10 hPa. In the lower mesosphere (78–82 km) (**Fig. 5b),** a different feature of the zonal winds was noted in the mid-latitudes; the zonal winds weakened but did not reverse on the SSW day. However, in the tropical (13°N) and polar (68°N) latitudes, the wind reversal started two weeks before the SSW day (around January 31) and attained peak values of around –24 m/s and –13 m/s, three and two days after the SSW day, respectively. Moreover, the polar lower mesospheric winds return eastward two days after their peak reversal, wherein tropical winds were observed a week after the peak reversal.

As clearly shown in **Fig. 5**, the mesospheric signatures to the SSW are more or less similar at the polar and tropical stations and different in the mid-latitudes. Moreover, the wind reversal in the upper mesosphere is greater in the mid-latitudes (**Fig. 5a**), lasting for more than a week. In the tropical and polar regions, wind reversal was noted after the SSW event for a short period. However, zonal wind oscillations were observed before the SSW event over the tropical station. At the tropical latitude, greater effects of the SSW were observed in the lower mesosphere (**Fig. 5b**), and peak reversal was noted (–24 m/s, the highest value of all stations) three days after the SSW event, lasting for a week. The delay and differences in the mesospheric wind reversal between the mid-latitudes and the polar- and tropical-latitudes may be attributed to PW forcing and mean circulation changes (Kodera, 2006; Eguchi and Kodera, 2007; Vargin and Kiryushov, 2019), as well as to middle atmospheric transport (Manney et al., 2015). Hence, the PW analysis of the MR measured winds may provide some clues for the delay in wind reversal.

3.4. Planetary waves in the mesosphere

To observe the PW activity in the mesosphere at all the observational stations during the 2018 SSW, the MR observed zonal winds during the 2017–2018 winter were subjected to wavelet analysis. We used "Morlet" wavelet analysis (Torrence and Compo, 1998) to estimate the wavelet spectrum. **Fig. 6** shows the wavelet spectra of the zonal winds averaged between 85–90 km in the upper mesosphere (**Fig.**

6a) and at 78–82 km in the lower mesosphere (**Fig. 6b**) for all four stations. The cone of influence is shown as a dashed black line, and the range of significant PW periods is shown with a thick contour line in the wavelet diagram, where the vertical line indicates the SSW day. From the wavelet spectra, it is evident that a wide spectrum of PWs (periods of ~2–4, 5–9, and 12–16 days) and intra-seasonal oscillation (ISO) period waves (~30–60 days) took place during the SSW winter from the polar to the tropical region at different time intervals.

The ISOs appeared at all stations at different times. The ISO was present well before the SSW day (from mid-December) in the upper mesosphere (**Fig. 6a**) and the polar and tropical latitudes, later gently disappearing after the SSW day. In contrast, in the mid-latitudes, the peak ISO amplitudes appeared during the SSW day, with higher amplitudes at CR than at KR, and persisted until the mid of March at the CR station. The strong ISOs are also noted in the lower mesosphere (**Fig. 6b)** at all the stations but showed different effects there. For instance, at the polar- and tropical-latitudes, they emerged well before (early January) the SSW day and continued until mid-March, whereas in the mid-latitudes, they attained peak amplitudes after the SSW day and continued until the end of March. The ISOs propagation and their effects on the mesosphere wind reversal have been discussed in the following sections.

In contrast, the 16-day, and 12–14 day PWs signatures are limited to only polar and tropical stations in the upper mesosphere (**Fig. 6a**). For instance, the 16-day PWs appeared from mid-December at the polar (68°N) station (ER) and vanished there before the SSW day. At the tropical station (14°N) (TR), 12–14 day PWs started appearing at the same time and faded off before the SSW day. This suggests that the zonal wind reversals (oscillations) both in the tropical and polar region before the SSW (January and early February) (**Fig. 5a**) could be due to the amplification of 12–16-day PWs and their interaction with the background mean flow. The occurrence of 16-day waves that are replaced by short-period PWs at high latitudes has been reported for other SSW years (Jacobi et al., 2003, 2016; Matthias et al., 2012).

Similar to ISOs, the 8-day-period (~5–9 days, peak at 8 days) PWs prevail at all the stations in the upper mesosphere (**Fig. 6a**). These waves showed distinct features in the upper mesosphere, although they appeared well before the SSW day in the mid and high latitudes, they attained peak amplitudes on the SSW day at CR and a few days (2–3 days) before at the ER and KR. However, at the tropical station (TR), they peaked 3–4 days after SSW. These PWs also exhibited their signature in the lower mesosphere; nevertheless,

they appeared at the tropical and polar stations during the SSW day and even well before the SSW day (mid-January (tropical) and late December (polar)) and disappeared (a very weak signal at KR) at the mid-latitude stations. In addition, small period (~2–4 days) PWs were also identified in the upper mesosphere in late December; however, their amplitudes were very small and are not considered in the present discussion.

Considering the mesospheric zonal wind reversal and the dominant PW periods from the polar to tropical region, the present SSW demands a further understanding of the latitudinal propagation of PWs, especially ISOs and 8-day waves, which appear at almost all stations. Moreover, the results in **Fig. 6** are evaluated based on single-point measurement. Hence, for more robust results we showed in **Fig.7a–b,** the latitudinal propagation of ISO and 8-day filtered zonal winds (10°–100°E covering all MR longitudes) at 80 km (maximum pressure level available in ERA5), respectively, from ERA5 reanalysis. The ability of ERA5 to detect SSW signatures in the lower mesosphere (up to 80 km) was already shown (**Fig. 4**), and the mesospheric zonal wind reversal is demonstrated at all stations, similar to the MR observations (**Fig. 3a**). Hence, it is appropriate to use ERA5 data for further analysis of ISOs and 8-day PWs to quantify the MR observed wave features. Here, we applied harmonic filtering analysis using the least-squares method (Giarnetti et al., 2015) to obtain the ISO and 8-day PW amplitudes. The advantage of harmonic analysis relative to the conventional filtering method is that the noise associated with multiple waves within the filtering band and the phase distortion due to nonlinear wave-wave interactions can be minimized. Here, the amplitude of the 8-day wave was obtained using harmonic analysis, considering periods between 6 and 10 days at a 1-day interval. Meanwhile, to obtain the ISO amplitudes, periods between 30 and 60 days were considered at an interval of 10 days, followed by the use of the least-squares method to obtain the amplitude of the best-fit harmonic in the chosen band.

It is evident from **Fig. 7(a)** that the ISO features appeared well before the SSW at all latitudes, and showed strong signatures at the mid-latitudes even after the SSW day. This agrees with the wavelet spectra obtained using the MR observations at the CR (51°N) and KR (56°N) stations (**Fig. 6**). It is also interesting to note that the ISO phase propagates from high (~60°N) to low latitudes (up to ~20°N) (black arrows in **Fig. 7a**), demonstrating the change in the meridional propagation of winds during SSW. The strong westward flows associated with the ISO could decelerate the mean eastward wind, thereby modifying them to proceed westward (wind reversal), as observed in **Fig. 5**. However, because the radar measures wind

at a point location, it is sometimes difficult to observe such progressive changes in wind reversal in accordance with ISO propagation. Another interesting point to be noted from **Fig. 7** is the 8-day wave (**Fig. 7b**) phase propagation, which propagates in contrast to the ISO, i.e., from low to high-latitudes (black arrows in **Fig. 7b**); higher amplitudes of the 8-day wave were observed in the polar region (60–90°N) from February 1 to the SSW day. Therefore, it is exciting to see how the combination of the ISO and 8-day waves modify the structure of the mean background winds through constructive and destructive interference in the mesosphere during the progression of SSW. A composite of the ISO and 8-day waves together is shown in **Fig. 7c**. It can be seen that the ISO amplitude is quite strong relative to the 8-day wave; therefore, the strong westward winds along with the ISO amplitudes have a stronger impact in modifying the mean background winds than do the 8-day waves.

Fig. 7c shows that the interference of ISO and 8-day waves results in westward winds in the mid-latitudes (40°–60°N) until before the SSW; in contrast, they appeared during and after the SSW day in the polar latitudes (60°–90°N). However, the resulting westward winds (ISO+8-day) (**Fig. 7c**) shifted down from the mid-latitudes, and the shift can be perceived between 40°N and 20°N during and after the SSW (around February 6–20). The westward winds (ISO+8-day) moved further up to the tropical latitudes after the SSW, but they are weak at the tropical latitudes. Moreover, the westward 8-day waves are observed after the SSW over the tropical latitudes (**Fig. 7b**), hence the wind delay in the tropics could be associated with both equatorward ISOs and 8-day PWs. Besides, the strong westward PWs (either ISO or combination) identified over the mid-latitudes (CR, KR) might provide the necessary feedback for zonal wind reversal on the SSW day. However, at the polar station (ER), the westward force of the ISO or the combination is weak and exists after the SSW day; hence, the wind reversal might be delayed. Henceforth, it is suggested that, although strong ISOs were recognized over the mid-latitudes, their direction of propagation (east or west) may change with height. For instance, at ~80 km (**Fig. 7a** and **7c**), although there are ISOs, winds are weak westward (or turn eastward), hence, radar observed winds in the lower mesosphere (**Fig. 5b**) showed only wind weakening in the mid-latitudes but not wind reversal. In any case, the ISOs have a strong effect on the mid-latitude zonal winds during the SSW.

Fig. 7, therefore**,** suggests that the PWs of ISO periods show greater effects on the zonal wind reversal between the latitudes 20°N and 60°N, owing to their westward flow; meanwhile, at high latitudes (above 60°N), 8-day PWs are responsible for the zonal wind reversal, where the westward ISO flow is weak and 8-day wave amplitudes are higher. At the tropical latitudes, weak ISOs and

8-day PWs are noted after the SSW. Moreover, the relative phase of the composite wave (ISO + 8-day) is the same in the tropics and the polar latitudes ($> 60^{\circ}$N) and different in the mid-latitudes, which could be responsible for the different timing of the wind reversal between the tropical/polar latitudes and the mid-latitudes.

In addition, the 8-day wave has some influence in decelerating the westward winds associated with the ISO due to destructive interference, which is seen in the low-latitudes. For instance, from **Fig. 7b** it is quite clear that the amplitude of the 8-day wave is opposite (i.e., eastward) that of the ISO amplitudes during the SSW day from the low-latitudes up to 40°N. The westward winds associated with the ISO between the latitudes 20°–40°N are greater than 25 m/s during the SSW day (**Fig. 7a**); meanwhile, eastward winds of nearly 5–8 m/s are associated with the 8-day wave (**Fig. 7b**), while resulting in a reduction in the westward winds of $>$ –20 m/s. This feature can be seen in **Fig. 7c** between 20°–40°N and shifted to the tropical latitudes after the SSW day. Hence, the propagations of the ISO and 8-day waves have a strong influence on the mean winds, with a major contribution from the ISO.

The question arises as to what kind of PWs and mechanism is responsible for the tropical (14°N) mesospheric higher wind reversal, as the observed ISOs (**Fig. 7a**) and ISO and 8-day composite (**Fig. 7c**) are observed to be a weak signal. Therefore, the wind reversal observed in the tropical mesosphere may be partly due to the ISO or the composite of ISO+8-day waves, and a major contribution from the other PWs. The existence of the PWs in the mesospheric altitudes in the tropical atmosphere is further controlled by the background winds and low-frequency climatic modes such as tropical QBO (Niranjan Kumar et al., 2011; Niranjan Kumar et al., 2019), which needs to be further investigated with extended analysis.

Briefly, the MR network observations in the mesosphere in association with the ERA5 demonstrates striking features of wave activity during the 2018 major SSW:

1) A wide spectrum of waves (8-day, 12–16-day, and ISO periods (30–60-day)) were observed from the tropical to the extra-tropical regions, 2) The signature of ISO was observed at all latitudes before the SSW day and continued in the mid-latitudes even after the SSW day, a weak signal of ISOs observed after the SSW over the tropical and polar latitudes. 3) The equatorward phase propagation of ISO and contrasting phase propagation of 8-day PWs were observed, the ISO propagation establishes the change in the meridional propagation, which in turn designates the changes in the mean mesospheric meridional circulation. 4) The time evaluation and phase propagation of ISO suggests that ISOs might be in-situ generated by various mechanisms (e.g., wave-wave interaction, mesospheric wind shear instabilities) in the mid-latitudes. 5) We speculate that the combined effect of dominant ISO and 8-day wave propagation and their relative phase caused the zonal wind reversal and its variations at the tropical and polar latitudes. 6) Further, it is interesting that the significant 8-day waves in the

lower mesosphere were observed only at the tropical and polar stations during the peak SSW but were weak/not significant in the mid-latitudes. This, in turn, suggests that the wind reversal in the lower mesosphere (**Fig. 5b**) might be influenced by the 8-day waves in the polar-, and the tropical region. In the mid-latitudes, wind weakening (**Fig. 5b**) is observed rather than wind reversal, owing to the weakness or absence of 8-day waves over the mid-latitudes.

It is worth mentioning that, for the first time, we have ascribed the mesospheric wind reversals as caused by ISO period oscillations rather than the classical high-frequency PWs and described their role in the lateral coupling of the mesosphere.

4. Conclusions

We described the polar to a tropical teleconnection in the mesosphere during the 2018 major SSW in the NH using simultaneous observations of an MR network. We used the Tirupati MR (13.63°N, 79.4°E) at the tropical station, Collm (51°N, 13°E) and Kazan (56°N, 49°E) MRs in the mid-latitudes, and Esrange (67.88°N, 21.07°E) MR in the polar region. We also utilized ERA5 data to describe the SSW characteristics and ISO and PW latitudinal propagation. The timing of the mesospheric zonal wind reversals and the analysis of planetary-scale waves with the intra-seasonal period at these radar stations were utilized to establish the connection between the tropical and extra-tropical mesosphere and to show the possible mean circulation changes. To the best of our knowledge, this is the first report on the observational evidence of intra-seasonal variability latitudinal coupling during the 2018 major SSW in the NH, rather than considering conventional 16-day waves. The main findings are summarized as follows.

1. The zonal wind reversal in the upper mesosphere (85–90 km) occurred on the peak SSW day in the mid-latitudes with a maximum value of ~ (–16) m/s, whereas in the tropical- and high-latitude regions, the reversal occurred two days after the SSW day with a peak value of –13 m/s, and –18 m/s, respectively. In the lower mesosphere (78–82 km), the mid-latitude zonal winds weakened but did not reverse, however, at the tropical/polar regions, the reversal started two weeks before the SSW day and attained a peak value (~ –24 m/s, –13 m/s) three and two days after the SSW, respectively. Hence, the highest zonal wind reversal during 2018 SSW was noted in the tropical lower mesosphere with a maximum value of ~ –24 m/s.

2. The wavelet analysis of zonal winds both in the upper and lower mesosphere at the four observational stations shows the presence of a wide spectrum of PWs (~2–4 days, 8 days, 12–16 days) and waves with an intra-seasonal period (30-60-day) oscillations. The signatures of 16-day waves at the polar and 12–14-day PWs in the tropical region in the upper-mesosphere were observed well before the SSW but dissipated before the peak SSW. The 8-day PWs were observed at all the stations in the upper mesosphere during the SSW, while in the lower mesosphere, they present only at the tropical and polar stations and disappear at the mid-latitudes.

3. The radar observations showed that the ISOs were observed before the peak SSW at all stations in the upper and lower mesosphere; however, at the mid-latitudes, they attained peak amplitude after the SSW day. The latitudinal propagation of both ISOs and 8-day waves using ERA5 suggests that the ISO phase propagated to low latitudes (up to 20°N) from 60°N, before the SSW. Reverse-phase propagation of the 8-day PWs was observed from the tropical to the polar regions. The superposition of these opposite phase propagation results in wind reversal in the mesosphere. The ISO, 8-day wave composite showed significant effects on the mesosphere wind reversal at the polar, mid-, and low-latitudes in different time intervals and caused the delay of wind reversal both at the polar and tropical stations.

4. The ISO propagation from 60°N-to-tropical regions during the SSW shows an indication of the reversed mean mesosphere meridional circulation during the SSW.

Our study suggests that major SSW in 2018 significantly affected the mesosphere from the polar to the tropical regions. Although several theoretical studies have proposed changes in the mean circulation during major SSWs, observational evidence in the mesosphere is very sparse. The present study using the MR network and ERA5 data attempted to reveal the impact of the 2018 major SSW at the tropical and extra-tropical stations and observed changes in the PWs and ISO propagation, including changes in the mean mesospheric circulation. Further studies are required to address the latitudinal and longitudinal propagation of ISOs in the upper mesosphere, using multiple observations, and model simulations.

Acknowledgments

This work was supported by the Korea Meteorological Administration (KMA) Research and Development Program under Grant KMI2020-01114, and Korea Polar Research Institute (PE19020), South Korea. Collm and Kazan wind observations have been supported by DFG through grant JA 836/38-1 and by RFBR through grant 18-505-12048.

The MR network data can be accessed with the following DOI link;

https://doi.org/10.5281/zenodo.3690723

The authors also thank the ERA5 team for providing the wind and temperature data used in the present study. The ERA5 datasets provided by the European Centre for Medium-Range Weather Forecasts (ECMWF) are publicly available at;

https://www.ecmwf.int/en/forecasts/datasets.

References

Andrews, D. G., Holton, J. R., and Leovy, C. B. (1987), Middle Atmosphere Dynamics, 489 pp., Academic, San Diego, Calif.

Anstey, J. A., & Shepherd, T. G. (2014). High-latitude influence of the quasi-biennial oscillation. Quarterly Journal of the Royal Meteorological Society,140(678), 1–21.

Baldwin, M. P., Ayarzagüena, B., Birner, T., Butchart, N., Butler, A. H., Charlton-Perez, A. J., Domeisen, D. I. V., Garfinkel, C. I., Garny, H., Gerber, E. P., Hegglin, M. I., Langematz, U., & Pedatella, N. M. (2021). Sudden Stratospheric Warmings. In Reviews of Geophysics (Vol. 59, Issue 1). Blackwell Publishing Ltd. https://doi.org/10.1029/2020RG000708

Butler, A. H., & Gerber, E. P. (2018). Optimizing the Definition of a Sudden Stratospheric Warming. *Journal of Climate*, *31*(6), 2337–2344. https://doi.org/10.1175/JCLI-D-17-0648.1

Butler, A. H., Lawrence, Z. D., Lee, S. H., Lillo, S. P., & Long, C. S. (2020). Differences between the 2018 and 2019 stratospheric polar vortex split events. *Quarterly Journal of the Royal Meteorological Society*, *146*(732), 3503–3521. https://doi.org/10.1002/qj.3858

Butler, A. H., Sjoberg, J. P., Seidel, D. J., & Rosenlof, K. H. (2017). A sudden stratospheric warming compendium. *Earth System Science Data*, *9*(1), 63–76. https://doi.org/10.5194/essd-9-63-2017

Chandran, A., & Collins, R. L. (2014). Stratospheric sudden warming effects on winds and temperature in the middle atmosphere at middle and low latitudes: a study using WACCM. *Annales Geophysicae*, *32*(7), 859–874. https://doi.org/10.5194/angeo-32-859-2014

Delhasse, A., Kittel, C., Amory, C., Hofer, S., & Fettweis, X. (2019). *Brief communication: Interest of a regional climate model against ERA5 to simulate the near-surface climate of the Greenland ice sheet* (preprint). Ice sheets/Greenland. https://doi.org/10.5194/tc-2019-96

Eguchi, N., & Kodera, K. (2007). Impact of the 2002, Southern Hemisphere, stratospheric warming on the tropical cirrus clouds and convective activity: SUDDEN WARMING AND TROPICAL CIRRUS. *Geophysical Research Letters*, *34*(5). https://doi.org/10.1029/2006GL028744

Eswaraiah, S., Kim, J.-H., Lee, W., Hwang, J., Kumar, K. N., & Kim, Y. H. (2020). Unusual Changes in the Antarctic Middle Atmosphere During the 2019 Warming in the Southern Hemisphere. *Geophysical Research Letters*, *47*(19). https://doi.org/10.1029/2020GL089199

Eswaraiah, S., Kim, Y. H., Hong, J., Kim, J.-H., Ratnam, M. V., Chandran, A., et al. (2016). Mesospheric signatures observed during 2010 minor stratospheric warming at King Sejong Station (62°S, 59°W). Journal of Atmospheric and Solar-Terrestrial Physics, 140,55–64. https://doi.org/ 10.1016/j.jastp.2016.02.007

Eswaraiah, S., Kim, Y. H., Lee, J., Ratnam, M. V., & Rao, S. V. B. (2018). Effect of Southern Hemisphere Sudden Stratospheric Warmings on Antarctica

Mesospheric Tides: First Observational Study. *Journal of Geophysical Research: Space Physics*. https://doi.org/10.1002/2017JA024839

Eswaraiah, S., Kim, Y. H., Liu, H., Ratnam, M. V., & Lee, J. (2017). Do minor sudden stratospheric warmings in the Southern Hemisphere (SH) impact coupling between stratosphere and mesosphere–lower thermosphere (MLT) like major warmings? Earth, Planets and Space, 69(1), 119. https://doi.org/10.1186/s40623-017-0704-5

Eswaraiah, S., Venkat Ratnam, M., Kim, Y. H., Kumar, K. N., Venkata Chalapathi, G., Ramanajaneyulu, L., et al. (2019). Advanced meteor radar observations of mesospheric dynamics during 2017 minor SSW over the tropical region. *Advances in Space Research*, *64*(10), 1940–1947. https://doi.org/10.1016/j.asr.2019.05.039

Eswaraiah, S., Venkat Ratnam, M., Krishna Murthy, B. v., & Vijaya Bhaskara Rao, S. (2011). Low-latitude mesospheric vertical winds observed using VHF radar. *Journal of Geophysical Research Atmospheres*, *116*(22). https://doi.org/10.1029/2011JD016385

Fahimi, S., Ahmadi-Givi, F., Mazraeh Farahani, M., & Meshkatee, A. H. (2021). Investigation of the relationship between Euro-Atlantic and West Asia blockings and major stratospheric sudden warmings in the period of 1959–2018. *Dynamics of Atmospheres and Oceans*, *95*. https://doi.org/10.1016/j.dynatmoce.2021.101245

Garfinkel, C. I., Son, S. W., Song, K., Aquila, V., & Oman, L. D. (2017). Stratospheric variability contributed to and sustained the recent hiatus in Eurasian winter warming. *Geophysical Research Letters*, *44*(1), 374–382. https://doi.org/10.1002/2016GL072035

Giarnetti, S., Leccese, F., & Caciotta, M. (2015). Non recursive multiharmonic least squares fitting for grid frequency estimation. Measurement: Journal of the International Measurement Confederation, 66, 229–237. https://doi.org/10.1016/j.measurement.2015.02.021

Harvey, V. L., Randall, C. E., Becker, E., Smith, A. K., Bardeen, C. G., France, J. A., & Goncharenko, L. P. (2019). Evaluation of the Mesospheric Polar Vortices in WACCM. *Journal of Geophysical Research: Atmospheres*, *124*(20), 10626–10645. https://doi.org/10.1029/2019JD030727

Hersbach, H., Bell, B., Berrisford, P., Hirahara, S., Horányi, A., Muñoz-Sabater, J., Nicolas, J., Peubey, C., Radu, R., Schepers, D., Simmons, A., Soci, C., Abdalla, S., Abellan, X., Balsamo, G., Bechtold, P., Biavati, G., Bidlot, J., Bonavita, M., … Thépaut, J. N. (2020). The ERA5 global reanalysis. *Quarterly Journal of the Royal Meteorological Society*, *146*(730), 1999–2049. https://doi.org/10.1002/qj.3803

Hersbach, H.,and Dee.,D(2016), ERA5 reanalysis is in production. ECMWF Newsletter No. 147 – Spring 2016, p. 7.

Hoffmann, P., Singer, W., Keuer, D., Hocking, W. K., Kunze, M., & Murayama, Y. (2007). Latitudinal and longitudinal variability of mesospheric winds and temperatures during stratospheric warming events. *Journal of Atmospheric and Solar-Terrestrial Physics*, *69*(17–18), 2355–2366. https://doi.org/10.1016/j.jastp.2007.06.010

Holton, J. R., & Tan, H.-C. (1980). The influence of the equatorial quasi-biennial oscillation on the global circulation at 50 mb. Journal of the Atmospheric Sciences,37(10), 2200–2208.

Huang, K. M., Xi, Y., Wang, R., Zhang, S. D., Huang, C. M., Gong, Y., & Cheng, H. (2019). Signature of a Quasi 30-Day Oscillation at Midlatitude Based on Wind Observations from MST Radar and Meteor Radar. *Journal of Geophysical Research: Atmospheres*, *124*(21), 11266–11280. https://doi.org/10.1029/2019JD031170

Jacobi, C., Arras, C., Geißler, C., & Lilienthal, F. (2019). Quarter diurnal signature in sporadic E occurrence rates and comparison with neutral wind shear. *Annales Geophysicae*, *37*(3), 273–288. https://doi.org/10.5194/angeo-37-273-2019

Jacobi, Ch. (2012), 6 year mean prevailing winds and tides measured by VHF meteor radar over Collm (51.3°N, 13.0°E), *J. Atmos. Sol.-Terr. Phys.,* 78-79, 8-18, https://doi.org/10.1016/j.jastp.2011.04.010.

Jacobi, Ch., Kürschner, D., Muller, H. G., Pancheva, D., Mitchell, N. J., & Naujokat, B. (2003). Response of the mesopause region dynamics to the February 2001 stratospheric warming. *Journal of Atmospheric and Solar-Terrestrial Physics*, *65*(7), 843–855. https://doi.org/10.1016/S1364-6826(03)00086-5

Jacobi, Ch., Samtleben, N., & Stober, G. (2016). Meteor radar observations of mesopause region long-period temperature oscillations. *Advances in Radio Science*, *14*, 169–174. https://doi.org/10.5194/ars-14-169-2016

Karpechko, A. Y., Charlton-Perez, A., Balmaseda, M., Tyrrell, N., & Vitart, F. (2018). Predicting Sudden Stratospheric Warming 2018 and Its Climate Impacts With a Multimodel Ensemble. *Geophysical Research Letters*, *45*(24), 13,538-13,546. https://doi.org/10.1029/2018GL081091

Kishore Kumar, G., Venkat Ratnam, M., Patra, A. K., Jagannadha Rao, V. V. M., Vijaya Bhaskar Rao, S., Kishore Kumar, K., et al. (2008). Low-latitude mesospheric mean winds observed by Gadanki mesosphere-stratosphere-troposphere (MST) radar and comparison with rocket, High Resolution Doppler Imager (HRDI), and MF radar measurements and HWM93. *Journal of Geophysical Research*, *113*(D19), D19117. https://doi.org/10.1029/2008JD009862

Kodera, K. (2006), Influence of stratospheric sudden warming on the equatorial troposphere, *Geophys. Res. Lett.*, *33*(6), 1–4, doi:10.1029/2005GL024510.

Korotyshkin, D., E. Merzlyakov, C. Jacobi, F. Lilienthal, and Q. Wu (2019b), Longitudinal MLT wind structure at higher mid-latitudes as seen by meteor

radars at central and Eastern Europe (13°E/49°E), *Adv. Sp. Res.*, 1–13, doi:10.1016/j.asr.2019.01.036.

Korotyshkin, D., Merzlyakov, E., Sherstyukov, O., & Valiullin, F. (2019). Mesosphere/lower thermosphere wind regime parameters using a newly installed SKiYMET meteor radar at Kazan (56°N, 49°E). *Advances in Space Research*, *63*(7), 2132–2143. https://doi.org/10.1016/j.asr.2018.12.032

Kozubek, M., Lastovicka, J., & Krizan, P. (2020). Comparison of key characteristics of remarkable ssw events in the southern and northern hemisphere. *Atmosphere*, *11*(10). https://doi.org/10.3390/atmos11101063

Krüger, K., Naujokat, B., & Labitzke, K. (2005). The Unusual Midwinter Warming in the Southern Hemisphere Stratosphere 2002: A Comparison to Northern Hemisphere Phenomena. J. Atmos. Sci., 62, 603–613, 2005.

Laskar, F. I., Chau, J. L., Stober, G., Hoffmann, P., Hall, C. M., & Tsutsumi, M. (2016). Quasi-biennial oscillation modulation of the middle- and high-latitude mesospheric semidiurnal tides during August-September: QBO MODULATION OF SEMIDIURNAL TIDES. *Journal of Geophysical Research: Space Physics*, *121*(5), 4869–4879. https://doi.org/10.1002/2015JA022065

Laskar, F. I., McCormack, J. P., Chau, J. L., Pallamraju, D., Hoffmann, P., & Singh, R. P. (2019). Interhemispheric Meridional Circulation During Sudden Stratospheric Warming. *Journal of Geophysical Research: Space Physics*, *124*(8), 7112–7122. https://doi.org/10.1029/2018JA026424

Liu, G., Huang, W., Shen, H., Aa, E., Li, M., Liu, S., & Luo, B. (2019). Ionospheric Response to the 2018 Sudden Stratospheric Warming Event at Middle- and Low-Latitude Stations Over China Sector. *Space Weather*, *17*(8), 1230–1240. https://doi.org/10.1029/2019SW002160

Lu, H., Hitchman, M. H., Gray, L. J., Anstey, J. A., & Osprey, S. M. (2020). On the role of Rossby wave breaking in the quasi-biennial modulation of the stratospheric polar vortex during boreal winter. *Quarterly Journal of the Royal Meteorological Society*, *146*(729), 1939–1959. https://doi.org/10.1002/qj.3775

Lu, H., Pancheva, D., Mukhtarov, P., & Cnossen, I. (2012). QBO modulation of traveling planetary waves during northern winter: QBO MODULATION OF TRAVELING WAVES. *Journal of Geophysical Research: Atmospheres*, *117*(D9), n/a-n/a. https://doi.org/10.1029/2011JD016901

Lu, X., Wu, H., Chu, X., Oberheide, J., Mlynczak, M. G., & Russell, J. M. (2019). Quasi-Biennial Oscillation of Short-Period Planetary Waves and Polar Night Jet in Winter Antarctica Observed in SABER and MERRA-2 and Mechanism Study With a Quasi-Geostrophic Model. *Geophysical Research Letters*, *46*(22), 13526–13534. https://doi.org/10.1029/2019GL084759

Luo, J., Gong, Y., Ma, Z., Zhang, S., Zhou, Q., Huang, C., Huang, K., Yu, Y., & Li, G. (2021). Study of the Quasi 10-Day Waves in the MLT Region During

the 2018 February SSW by a Meteor Radar Chain. *Journal of Geophysical Research: Space Physics*, *126*(3). https://doi.org/10.1029/2020JA028367

Manney, G. L., Lawrence, Z. D., Santee, M. L., Read, W. G., Livesey, N. J., Lambert, A., et al. (2015). A minor sudden stratospheric warming with a major impact: Transport and polar processing in the 2014/2015 Arctic winter. *Geophysical Research Letters*, *42*(18), 7808–7816. https://doi.org/10.1002/2015GL065864

Matsuno, T. (1971), A dynamical model of the stratospheric sudden warming, J. Atmos. Sci., 28, 1479–1494.

Matthias, V., Hoffmann, P., Rapp, M., & Baumgarten, G. (2012). Composite analysis of the temporal development of waves in the polar MLT region during stratospheric warmings. *Journal of Atmospheric and Solar-Terrestrial Physics*, *90–91*, 86–96. https://doi.org/10.1016/j.jastp.2012.04.004

Medvedeva, I. V., Semenov, A. I., Pogoreltsev, A. I., & Tatarnikov, A. V. (2019). Influence of sudden stratospheric warming on the mesosphere/lower thermosphere from the hydroxyl emission observations and numerical simulations. *Journal of Atmospheric and Solar-Terrestrial Physics*, *187*, 22–32. https://doi.org/10.1016/j.jastp.2019.02.005

Mitchell, N. J., Pancheva, D., Middleton, H. R., and Hagan, M. E. (2002), Mean winds and tides in the Arctic mesosphere and lower thermosphere, *J. Geophys. Res. Sp. Phys.*, *107*(A1), doi:10.1029/2001JA900127.

Niranjan Kumar, K., Sharma, S. K., Joshi, V., & Ramkumar, T. K. (2019). Middle atmospheric planetary waves in contrasting QBO phases over the Indian low latitude region. *Journal of Atmospheric and Solar-Terrestrial Physics*, *193*, 105068. https://doi.org/10.1016/j.jastp.2019.105068

Niranjankumar, K., Ramkumar, T. K., & Krishnaiah, M. (2011). Vertical and lateral propagation characteristics of intra seasonal oscillation from the tropical lower troposphere to upper mesosphere, J. Geophys. Res., 116, D21112, doi:10.1029/2010JD015283.

Pedatella, N., Chau, J., Schmidt, H., Goncharenko, L., Stolle, C., Hocke, K., et al. (2018). How Sudden Stratospheric Warming Affects the Whole Atmosphere. *Eos*, *99*. https://doi.org/10.1029/2018EO092441

Quiroz, R. S. (1969), The warming of the upper stratosphere in February 1966 and the associated structure of the mesosphere, Mon. Wea. Rev., 97, 541–552.

Rao, J., Garfinkel, C. I., & White, I. P. (2020). Predicting the Downward and Surface Influence of the February 2018 and January 2019 Sudden Stratospheric Warming Events in Subseasonal to Seasonal (S2S) Models. *Journal of Geophysical Research: Atmospheres*, *125*(2). https://doi.org/10.1029/2019JD031919

Rao, S. V. B., Eswaraiah, S., Venkat Ratnam, M., Kosalendra, E., Kishore Kumar, K., Sathish Kumar, S., et al. (2014). Advanced meteor radar installed

at Tirupati: System details and comparison with different radars: Tirupati Enhanced Meteor Detection Radar. *Journal of Geophysical Research: Atmospheres*, *119*(21), 11,893-11,904. https://doi.org/10.1002/2014JD021781

Rüfenacht, R., Baumgarten, G., Hildebrand, J., Schranz, F., Matthias, V., Stober, G., et al. (2018). Intercomparison of middle-atmospheric wind in observations and models. *Atmospheric Measurement Techniques*, *11*(4), 1971–1987. https://doi.org/10.5194/amt-11-1971-2018

Sathishkumar, S., Sridharan, S., & Jacobi, Ch. (2009). Dynamical response of low-latitude middle atmosphere to major sudden stratospheric warming events. *Journal of Atmospheric and Solar-Terrestrial Physics*, *71*(8–9), 857–865. https://doi.org/10.1016/j.jastp.2009.04.002

Satterfield E.A. et al. (2022) Statistical Parameter Estimation for Observation Error Modelling: Application to Meteor Radars. In: Park S.K., Xu L. (eds) Data Assimilation for Atmospheric, Oceanic and Hydrologic Applications (Vol. IV). Springer, Cham. https://doi.org/10.1007/978-3-030-77722-7_8

Schwartz, C. and Garfinkel, C. I. (2017), Relative roles of the MJO and stratospheric variability in North Atlantic and European winter climate, J. Geophys. Res. Atmos., 122, 4184–4201, doi:10.1002/2016JD025829

Shepherd, M. G., Wu, D. L., Fedulina, I. N., Gurubaran, S., Russell, J. M., Mlynczak, M. G., & Shepherd, G. G. (2007). Stratospheric warming effects on the tropical mesospheric temperature field. *Journal of Atmospheric and Solar-Terrestrial Physics*, *69*(17–18), 2309–2337. https://doi.org/10.1016/j.jastp.2007.04.009

Shepherd, T. G., Polichtchouk, I., Hogan, R. J., & Simmons, A. J. (2018). Report on Stratosphere Task Force, (June), 32.

Shi, C., Xu, T., Guo, D., & Pan, Z. (2017). Modulating effects of planetary wave 3 on a stratospheric sudden warming event in 2005. Journal of the Atmospheric Sciences, 74(5), 1549–1559. https://doi.org/10.1175/JAS-D-16-0065.1

Stober, G., Kuchar, A., Pokhotelov, D., Liu, H., Liu, H.-L., Schmidt, H., et al. (2021). Interhemispheric differences of mesosphere–lower thermosphere winds and tides investigated from three whole-atmosphere models and meteor radar observations. *Atmospheric Chemistry and Physics*, *21*(18), 13855–13902. https://doi.org/10.5194/acp-21-13855-2021

Tarek, M., Brissette, F. P., & Arsenault, R. (2019). *Evaluation of the ERA5 reanalysis as a potential reference dataset for hydrological modeling over North-America* (preprint). Catchment hydrology/Modelling approaches. https://doi.org/10.5194/hess-2019-316

Torrence, C., and Compo., G. P. (1998), A practical guide to wavelet analysis, Bull. Amer. Meteorol. Soc., 79(1), 61–78, doi:10.1175/1520-0477(1998)079<0061:APGTWA>2.0.CO;2

van Loon, H., Jenne, R. L., & Labitzke, K. (1973). Zonal harmonic standing waves. *Journal of Geophysical Research*, *78*(21), 4463–4471. https://doi.org/10.1029/jc078i021p04463

Vargin, P. N., & Kiryushov, B. M. (2019). Major Sudden Stratospheric Warming in the Arctic in February 2018 and Its Impacts on the Troposphere, Mesosphere, and Ozone Layer. *Russian Meteorology and Hydrology*, *44*(2), 112–123. https://doi.org/10.3103/S1068373919020043

Vineeth, C., Kumar Pant, T., & Sridharan, R. (2009). Equatorial counter electrojets and polar stratospheric sudden warmings – a classical example of high latitude-low latitude coupling? *Annales Geophysicae*, *27*(8), 3147–3153. https://doi.org/10.5194/angeo-27-3147-2009

Vineeth, C., Pant, T. K., Kumar, K. K., & Sumod, S. G. (2010). Tropical connection to the polar stratospheric sudden warming through quasi 16-day planetary wave. *Annales Geophysicae*, *28*(11), 2007–2013. https://doi.org/10.5194/angeo-28-2007-2010

Wang, Y. et al. (2019), Winter 2018 major sudden stratospheric warming impact on midlatitude mesosphere from microwave radiometer measurements, *Atmos. Chem. Phys. Discuss.*, (2017), 1–26, doi:10.5194/acp-2018-1361.

White, I. P., Lu, H., Mitchell, N. J., & Phillips, T. (2015). Dynamical response to the QBO in the northern winter stratosphere: Signatures in wave forcing and eddy fluxes of potential vorticity. *Journal of the Atmospheric Sciences*, *72*(12), 4487–4507. https://doi.org/10.1175/JAS-D-14-0358.1

Zülicke, C., & Becker, E. (2013). The structure of the mesosphere during sudden stratospheric warmings in a global circulation model: MESOSPHERE STRUCTURE DURING STRATWARMS. *Journal of Geophysical Research: Atmospheres*, *118*(5), 2255–2271. https://doi.org/10.1002/jgrd.50219

Figure captions

Figure 1. Geographical location map of the advanced meteor radar network.

Figure 2. Time–altitude cross-sections of the (a) daily mean polar cap temperature at 80–90°N and (b) daily zonal mean zonal wind at 60°N obtained from ERA5. The approximate height of the corresponding pressure level is displayed on the right axis. (c) Planetary wave (k = 1 and k = 2) amplitudes at 10 hPa and 60°N. The vertical dashed lines indicate the day of peak warming, whereas the dashed horizontal lines in (a) and (b) indicate the 10 hPa pressure level.

Figure 3. (a) The time–height contour of the daily mean zonal wind obtained from 1 December 1, 2017, to 31 March 31, 2018, using Esrange radar (ER) at 68°N, Kazan meteor radar (KR) at 56°N, Collm meteor radar (CR) at 51°N, and Tirupati meteor radar (TR) at 14°N (top to bottom). (b) Same as (a) but shows the meridional winds. The vertical lines indicate the SSW day.

Figure 4. Time–height contours of the daily mean zonal winds obtained from

ERA5 data from December 1, 2017, to March 31, 2018, near meteor radar locations. The vertical line indicates the SSW day.

Figure 5. Daily mean variability of the averaged zonal winds (solid lines) (a) in the upper mesosphere (85–90 km), and in the (b) lower mesosphere (78–82km) was obtained using the meteor radar network. Daily mean zonal winds at 10 hPa, 60°N are shown by a dotted black line. The dashed horizontal line indicates the zero-wind level, and the vertical line indicates the SSW day.

Figure 6. Continuous wavelet spectra of the averaged zonal winds in the (a) upper mesosphere (85–90 km), (b) lower mesosphere (78–82km) were observed by the meteor radar network. The dashed curved black lines in the wavelet spectra show the respective cone of influence, and the vertical lines show the SSW day.

Figure 7. (a) 30–60-day filtered intra-seasonal oscillations (ISOs) of the zonal wind at 80 km using ERA5 data. (b) Same as (a) but for the 8-day wave, and (c) shows the composite of both ISO and 8-day waves. The filtered oscillations are obtained for the zonal wind between the longitudes 10 –100 E (covering all meteor radar longitudes). The dashed vertical lines show the SSW day.

Figures:

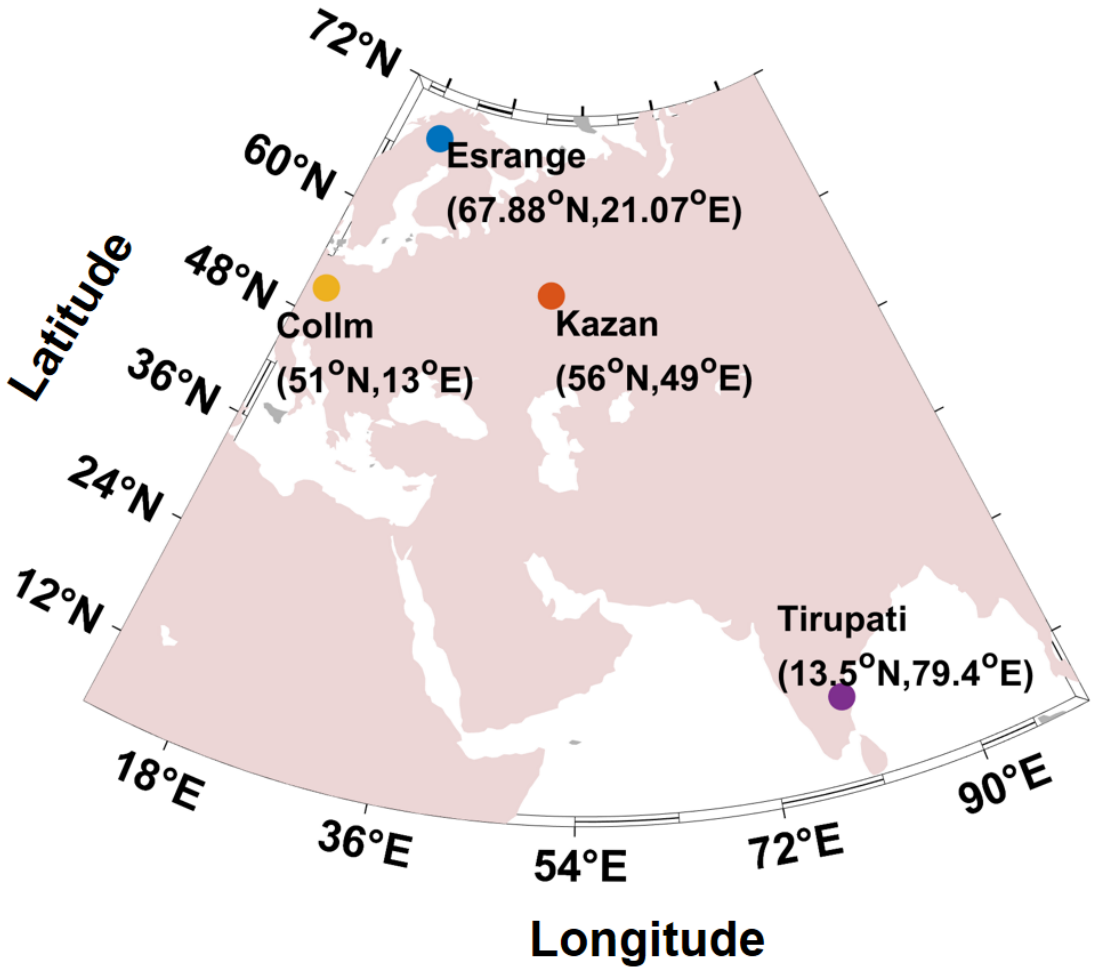

Figure 1. Geographical location map of the advanced meteor radar network.

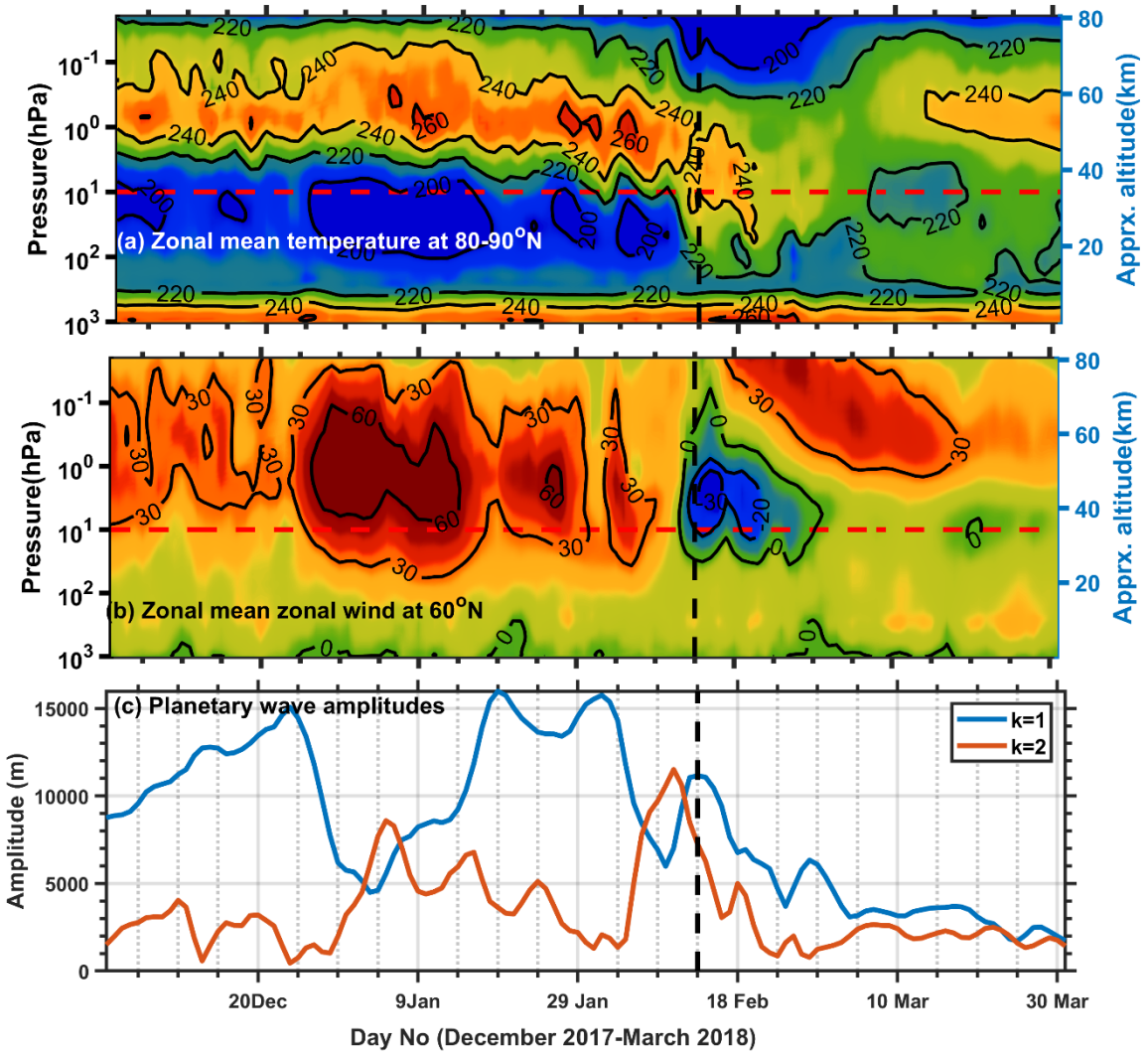

Figure 2. Time–altitude cross-sections of the (a) daily mean polar cap temperature at 80–90°N and (b) daily zonal mean zonal wind at 60°N obtained from ERA5. The approximate height of the corresponding pressure level is displayed on the right axis. (c) Planetary wave (k = 1 and k = 2) amplitudes at 10 hPa and 60°N. The vertical dashed lines indicate the day of peak warming, whereas the dashed horizontal lines in (a) and (b) indicate the 10 hPa pressure level.

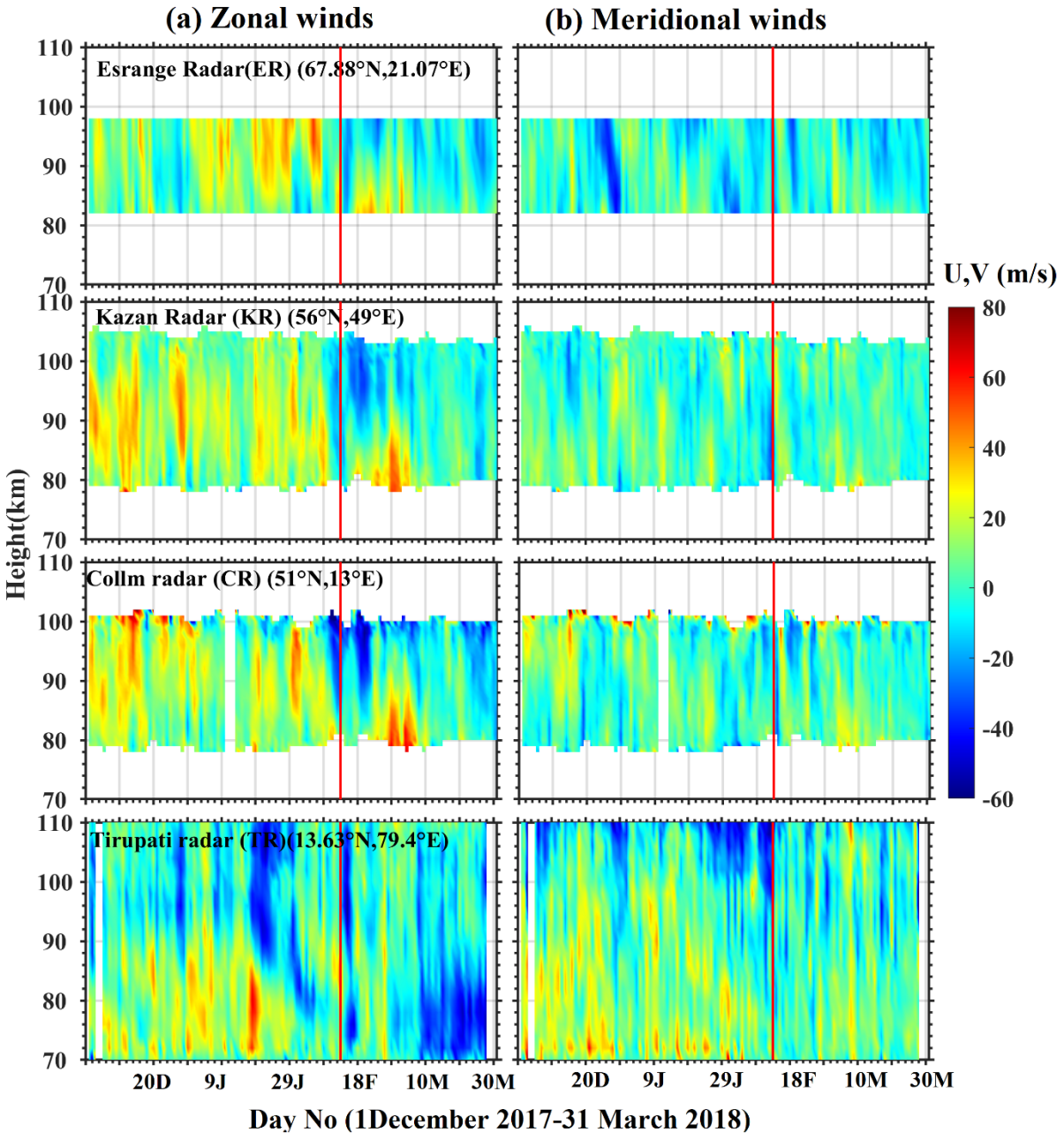

Figure 3. (a) The time–height contour of the daily mean zonal wind obtained from 1 December 1, 2017, to 31 March 31, 2018, using Esrange radar (ER) at 68°N, Kazan meteor radar (KR) at 56°N, Collm meteor radar (CR) at 51°N,

and Tirupati meteor radar (TR) at 14°N (top to bottom). (b) Same as (a) but shows the meridional winds. The vertical lines indicate the SSW day.

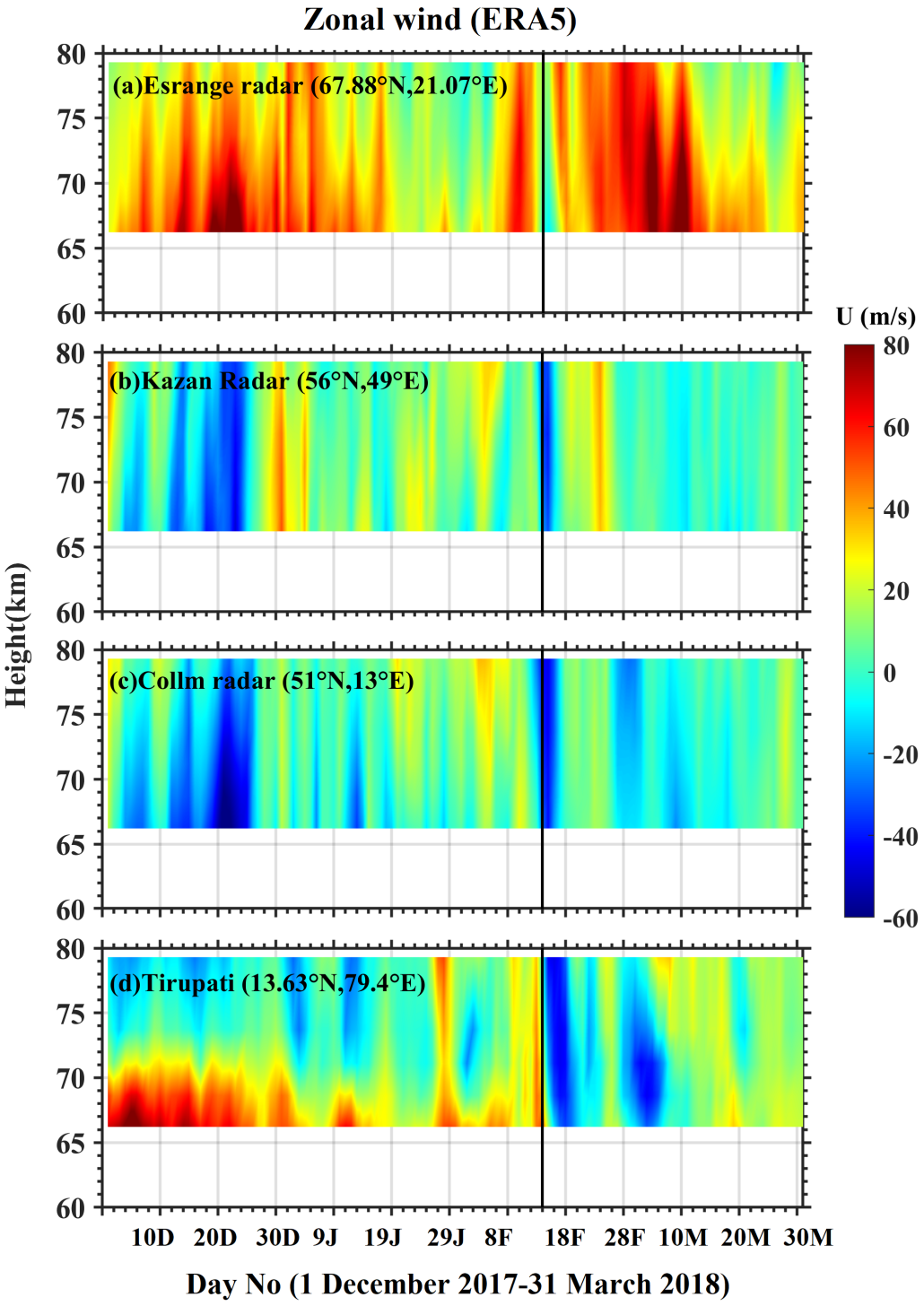
Zonal wind (ERA5)
(a)Esrange radar (67.88°N,21.07°E)
(b)Kazan Radar (56°N,49°E)
(c)Collm radar (51°N,13°E)
(d)Tirupati (13.63°N,79.4°E)
Height(km)
80
75
70
65
60
U (m/s)
80
60
40
20
0
-20
-40
-60
10D
20D
30D
9J
19J
29J
8F
18F
28F
10M
20M
30M
Day No (1 December 2017-31 March 2018)

Figure 4. Time–height contours of the daily mean zonal winds obtained from ERA5 data from December1, 2017, to March 31, 2018, near meteor radar locations. The vertical line indicates the SSW day.

Figure 5. Daily mean variability of the averaged zonal winds (solid lines) (a) in the upper mesosphere (85–90 km), and in the (b) lower mesosphere (78–82km) was obtained using the meteor radar network. Daily mean zonal winds at 10 hPa, 60°N are shown by a dotted black line. The dashed horizontal line indicates the zero-wind level, and the vertical line indicates the SSW day.

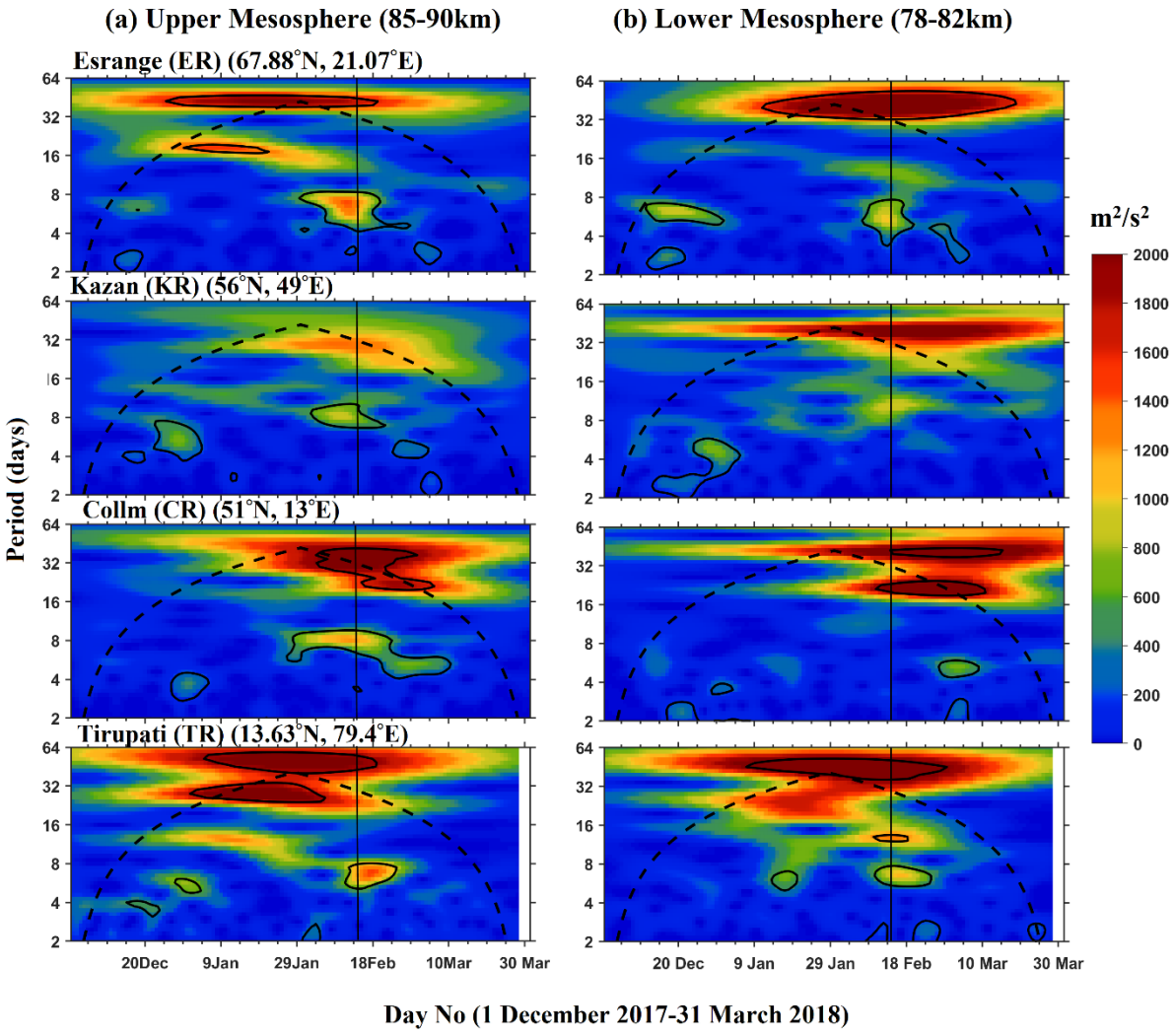

Figure 6. Continuous wavelet spectra of the averaged zonal winds in the (a) upper mesosphere (85–90 km), (b) lower mesosphere (78–82km) were observed by the meteor radar network. The dashed curved black lines in the wavelet

spectra show the respective cone of influence, and the vertical lines show the SSW day.

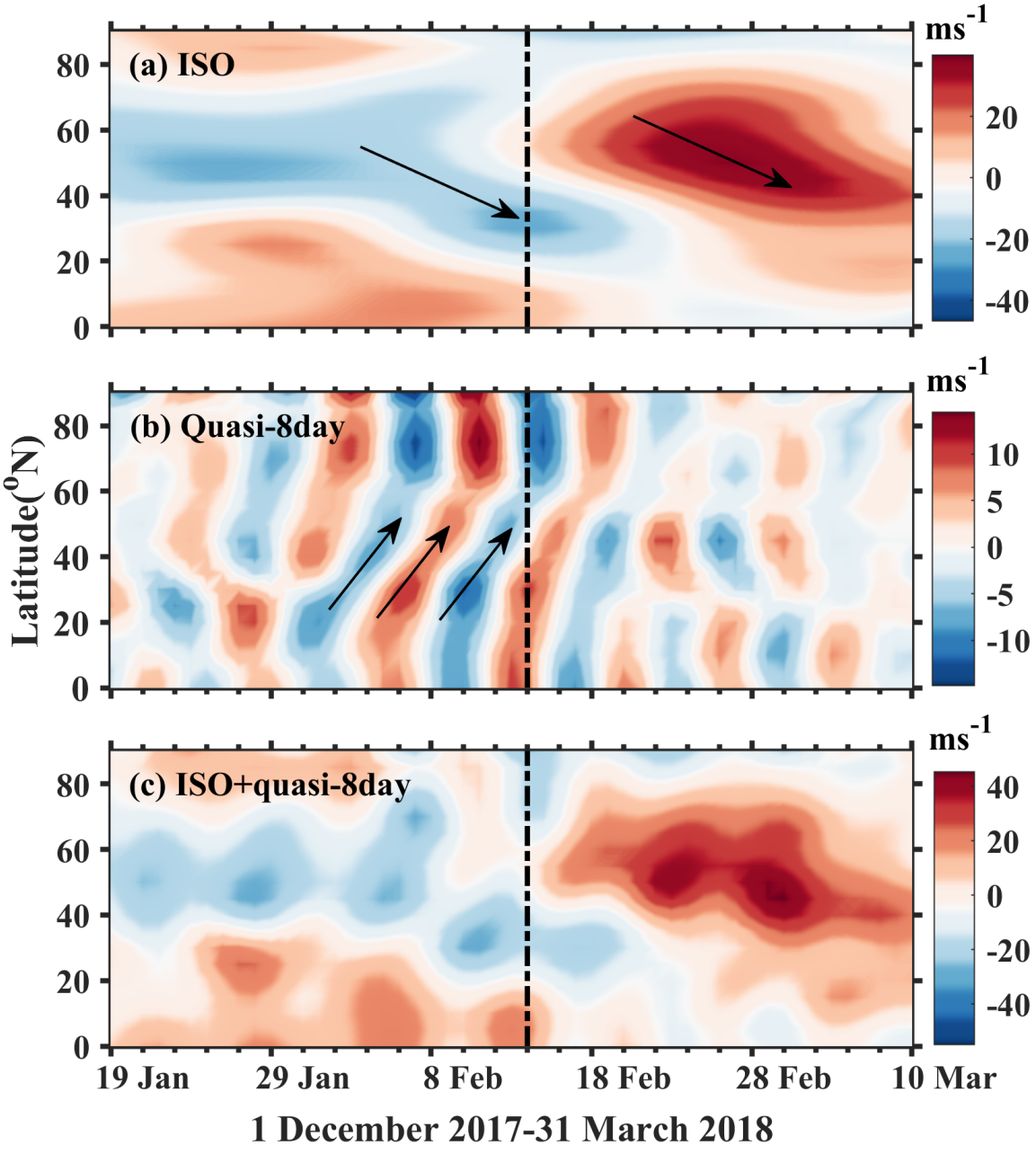

Figure 7. (a) 30–60-day filtered intra-seasonal oscillations (ISOs) of the zonal

wind at 80 km using ERA5 data. (b) Same as (a) but for the 8-day wave, and (c) shows the composite of both ISO and 8-day waves. The filtered oscillations are obtained for the zonal wind between the longitudes 10 –100 E (covering all meteor radar longitudes). The dashed vertical lines show the SSW day.